frontiers | Frontiers in Energy Research

ORIGINAL RESEARCH
published: 26 May 2022
doi: 10.3389/fenrg.2022.883972

High-Temperature Characterization of Melted Nuclear Core Materials: Investigating Corium Properties Through the Case Studies of In-Vessel and Ex-Vessel Retention

Jules Delacroix, Christophe Journeau and Pascal Piluso*

CEA, DES, IRESNE, DTN, Saint-Paul-Lez-Durance, France

During a severe accident in a nuclear reactor, the molten core—or corium—may be relocated into the reactor vessel's lower plenum in case of core support plate failure. The severe accident management strategy for In-Vessel Retention—or IVR—consists in stabilizing the corium within the reactor pressure vessel by external cooling of the vessel's lower head. If now, the vessel fails due to excessive thermal loading on its walls, the Ex-Vessel Retention—or EVR—strategy is adopted. In this case, the core melt stabilization can be achieved by effective corium spreading, either in the reactor vessel cavity or in a dedicated "core-catcher", and cooling by water. The success of both strategies highly depends on the corium behavior at high temperatures, conditioning vessel's integrity for IVR, and promotion for the spreading of the EVR. This involves a variety of fundamental mechanisms closely related to heat and mass transfer regimes prevailing at the system scale, which requires further analytical and experimental insight to determine the primary mechanisms and feed the modeling tools, allowing the numerical simulations of severe accident scenarios.

Within the framework of corium characterization at high temperatures, the present study aims at filling the lack of such fundamental data as density, surface tension, liquidus and solidus temperatures, and viscosity. In order to accurately measure these properties at high temperatures, the VITI facility is designed with various configurations. Concerning IVR, the influence of density and surface tension is particularly highlighted through VITI-SD and VITI-MBP configurations, and practical applications of experimental results are finally discussed, in link with the focusing effect issue at the thin upper metallic layer of the corium pool. Concerning EVR, the properties of interest are solidus/liquidus temperature and dynamic viscosity, and typical experimental results obtained through VITI-VPA and VITI-GFL configurations are discussed in view of characterizing corium spreading.

Keywords: corium, severe accident, high temperature, physical properties, in-vessel retention, ex-vessel retention, VITI experiment

OPEN ACCESS

Edited by:
Yapei Zhang,
Xi'an Jiaotong University, China

Reviewed by:
Huandong Chen,
Sun Yat-sen University, Zhuhai Campus, China
Luteng Zhang,
Chongqing University, China

****Correspondence:***
Jules Delacroix
jules.delacroix@cea.fr

Specialty section:
This article was submitted to Nuclear Energy, a section of the journal Frontiers in Energy Research

Received: *25 February 2022*
Accepted: *20 April 2022*
Published: *26 May 2022*

Citation:
Delacroix J, Journeau C and Piluso P (2022) High-Temperature Characterization of Melted Nuclear Core Materials: Investigating Corium Properties Through the Case Studies of In-Vessel and Ex-Vessel Retention. Front. Energy Res. 10:883972. doi: 10.3389/fenrg.2022.883972

1 INTRODUCTION

Following the Fukushima Daiichi accident, safety studies have been performed: families of initiators have been re-evaluated, and several assessment analyses have been performed, including response to severe accident conditions, mitigation tools, and coping time (Baek, et al., 2017; Song, 2021). International programs have been devoted to the understanding and modeling of the Fukushima Daiichi severe accident (Nakayoshi, et al., 2020; Pellegrini, et al., 2020).

Even if the overall severe accident phenomenology is relatively well-known, the complex coupling of physical mechanisms and their modeling involving corium progression can generate discrepancies for severe accident calculation assessment. As an example, let us mention the various calculations of the Fukushima Daiichi accident as predicted by different severe accident integral codes (Pellegrini, et al., 2016). Such discrepancies have been recently reduced by taking the same physical properties in all participating codes (Pellegrini, et al., 2022).

The lack of reliable knowledge of corium properties is certainly one of the major sources of uncertainties. This issue can be highlighted through the case study of the mitigation approaches called the In-vessel retention (IVR) (Bakuta, et al., 2015; Fichot, et al., 2020) and ex-vessel retention (EVR) (Journeau, et al., 2005) strategies. Specific severe accident phenomena such as fuel coolant interaction and steam explosion could damage the containment building and lead to fission product release. Accurate knowledge of corium properties has been identified as a major issue, which must be addressed to ensure reliable nuclear safety for pressurized water reactors (Piluso, et al., 2017).

During a severe accident in a nuclear reactor, the molten core—or corium—may be relocated into the reactor vessel's lower plenum in case of core support plate failure. Different Severe Accident Management (SAM) strategies have been proposed for the current fleet and new-built reactors in which the molten core retention is to be achieved either in-vessel or ex-vessel (Fischer, et al., 2016; Amidu, et al., 2022). The severe accident management strategy for IVR consists in stabilizing the corium within the Reactor Pressure Vessel (RPV) by external cooling of the vessel's lower head (Ma, et al., 2016). The success of the IVR strategy highly depends on corium behavior at the lower head scale. This behavior involves a variety of mechanisms in link with heat and mass transfer at the pool scale. Such phenomena may lead to the stratification of the corium pool, as observed in MASCA (Tsurikov, 2007) and RASPLAV (Asmolov and Tsurikov, 2000) experiments, performed in the framework of OECD projects, and CORDEB (Fichot, et al., 2022), an EU project. In particular, the formation of a "thin" light metal layer on top of the stratified corium pool, in direct contact with the vessel wall, may deeply alter corium pool topology. As shown hereafter, the so-called "focusing effect" (concentration of the heat flux in a thermally conductive metallic layer) is of primary interest regarding vessel integrity and requires further analytical and experimental insight to determine the fundamental mechanisms. A recent benchmark exercise (Carénini, et al., 2017) involving integral code-based sensitivity analyses has demonstrated the major impact of light metal layer properties. In this configuration, the sign of surface tension temperature coefficient $d\sigma/dT$ will play an important role in the Bénard–Marangoni current at the free surface atop the thin layer, impacting thus convection patterns, as shown hereafter.

In case IVR cannot be guaranteed, EVR is adopted. In the case of EVR through the Concrete Cavity [EVRCC, (Amidu, et al., 2022)], there are two options depending whether the cavity is filled or not by water at the time of the vessel melt-through. In the case of a wet cavity (Fischer, et al., 2016), the corium jet fragments, a process largely controlled by surface tension (Thakre, 2015), and forms a debris bed that will be cooled by the surrounding water. In addition, surface tension will also play an important role, for example, in oxide-metal ex-vessel configurations (stratification and emulsion). If water cooling is revealed to be impossible, the concrete basemat will be ablated because of continuing Molten Core Concrete Interaction (MCCI) (Farmer, et al., 2016). In case of an initially dry cavity, the MCCI starts and water flooding is activated with the goal of arresting concrete ablation (Bonnet, et al., 2017). For other types of nuclear reactors based on a so-called "core-catcher" approach, for example, the European Pressurized Reactor (EPR), the core melt stabilization is achieved by designing a core-catcher in a dedicated lateral compartment (Fischer, 2004). The melt discharge from the RV cavity to the core-catcher requires effective corium spreading before flooding to reduce the heat flux due to the corium decay heat. Spreading is controlled by the coupling of melt solidification with hydrodynamics through the evolution of its rheology (Journeau, 2006). It is, thus, of prime interest to determine the evolution of viscosity as a function of melt temperature and composition and characterizing accurately the different phase transitions experienced by corium mixtures.

Consequently, the previous observations enhance the necessity to access reliable measurements of density, surface tension, liquidus and solidus temperatures, and viscosity for achieving a consistent modeling of the actual corium flow topology. These issues are addressed in this study in order to bridge the gap between numerical simulations and actual corium thermal-hydraulics.

In the recent years, the VIscometer Temperature Installation (VITI) experimental facility of the CEA Cadarache PLINIUS prototypic corium platform (Journeau, et al., 2022) has been upgraded, conferring it the status of a versatile apparatus, dedicated to the investigation of fundamental phenomena linked to severe accident issues. Among other topics, this upgrade has made possible the high-temperature characterization of the corium properties of interest, each linked to a specific configuration of VITI. In this article, the unique capabilities of VITI are highlighted within the scope of both IVR and EVR. On the one hand, in **Section 2**, the focus is placed on the measurements of the surface tension and density of liquid metals at high temperatures for IVR through the VITI-SD and VITI-MBP configurations, respectively. The typical results that can be obtained are then discussed through the prism of the focusing effect issue. On the other hand, in **Section 3**, the case study of corium spreading is investigated for EVR, involving rather the solidus/liquidus temperatures and dynamic viscosity of

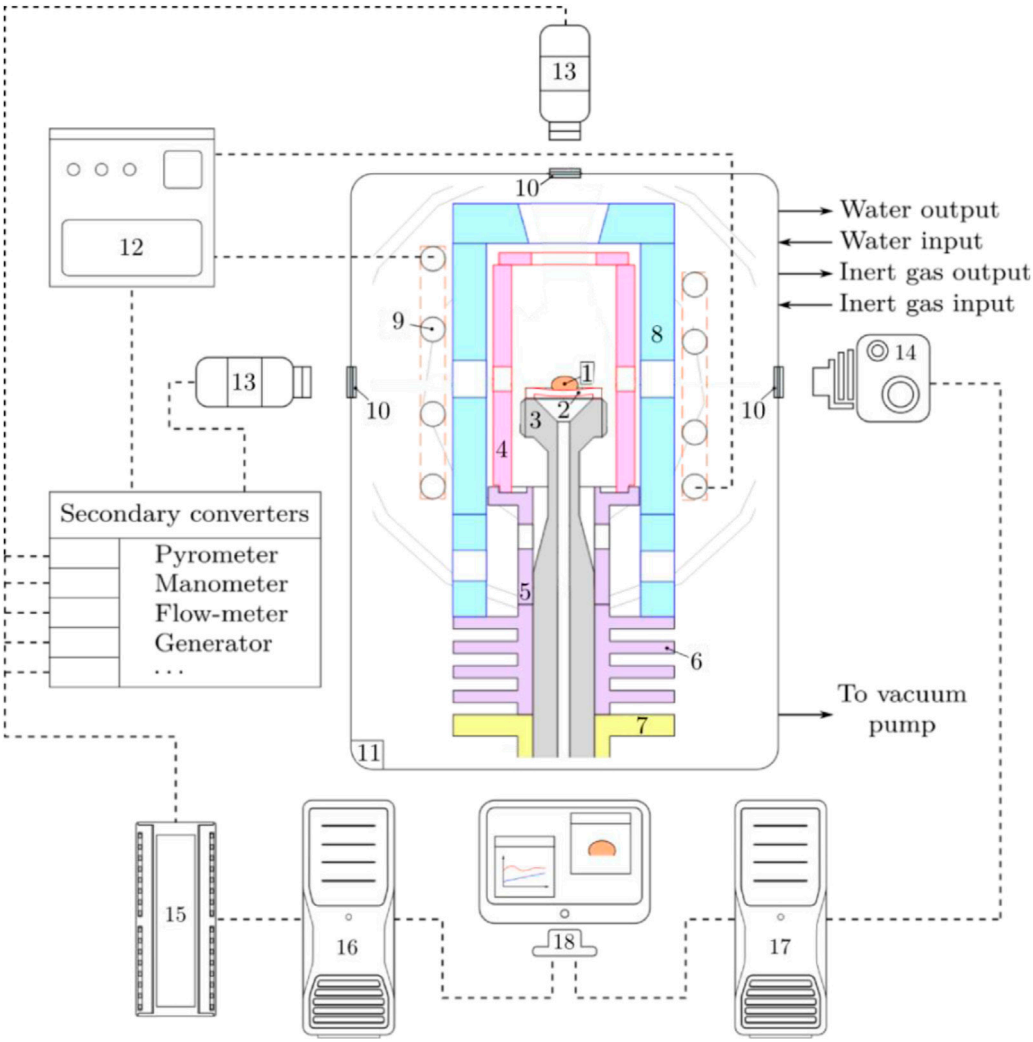

FIGURE 1 | Overall layout of VITI-SD configuration (Chikhi, et al., 2019). 1: liquid droplet; 2: substrate; 3: substrate support; 4: susceptor; 5: susceptor support; 6: fins; 7: global support; 8: thermal shield; 9: inductor; 10: windows; 11: confinement vessel; 12: generator; 13: pyrometers; 14: camera; 15: data bus; 16: acquisition PC; 17: imaging PC; 18: monitoring.

oxide mixtures that are measured through the VITI-VPA and VITI-GFL configurations, respectively.

2 MEASURING THE SURFACE TENSION AND DENSITY OF LIQUID METALS AT HIGH TEMPERATURES FOR IN-VESSEL RETENTION: THE VITI-SD AND VITI-MBP EXPERIMENTS

As previously introduced, in order to properly describe the thermal-hydraulics of the upper layer, there is a need for experimental data about the density and surface tension of liquid steels at high temperatures. In French PWR, the vessel is made of 304L austenitic stainless steel and 16MND5 (A508) ferritic steel, while the internal structure of the core is made of 316 and 304L austenitic stainless steel. Concerning surface tension, a review of the existing literature (Dubberstein, et al., 2015; Brooks, et al., 2005; Egry and Brillo, 2009; Matsumoto, et al., 2005) underlines a significant dispersion of surface tension measurements from both qualitative and quantitative viewpoints, in link with experimental uncertainties on σ, T, and the sample's composition. Concerning the latter, the major impact of such minor components as sulfur must be taken into account, given their potential influence on the evolution of $\sigma(T)$ (Mills, and Brooks, 1994). Moreover, to our knowledge, there seems to be no available data above the temperature of 1800°C, in link with the significant vaporization of steel occurring around this threshold temperature. Finally, for 16MND5-grade, the data are missing for both density and surface tension.

The VITI facility is used to provide such new data at high temperatures for the density and surface tension of the liquid

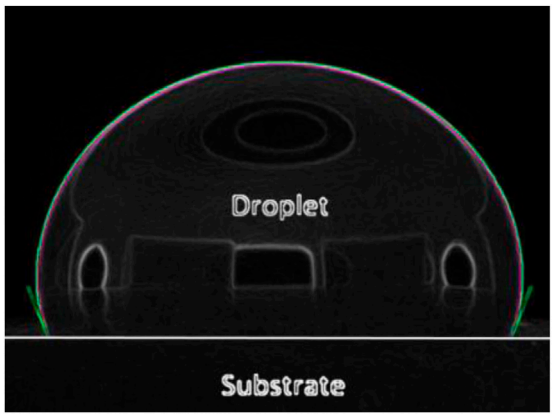

FIGURE 2 | Contour fitting—green line—of liquid steel sessile droplet.

steels of interest. On the one hand, the Sessile Droplet—SD—technique is used for the measurement of density ρ, and on the other hand, the Maximum Bubble Pressure—MBP—is used for the proper estimation of σ.

2.1 VITI-SD Configuration and Density Measurements

2.1.1 Experimental Layout

The VITI-SD general layout is displayed in **Figure 1**. The liquid droplet 1) rests on a dedicated plane substrate 2), made of yttria-stabilized zirconia, chosen for its chemical inertia with liquid steel at high temperature, and the drop-substrate system bears on the substrate support 3).

The whole system is heated by the so-called indirect induction method: the water-cooled inductor 9), connected to the power generator 12), is electromagnetically coupled with the so-called susceptor 4), which is supported by 5). The susceptor heats the sample up to the target temperature by radiative heat transfer. The thermal shield 8) is placed around the susceptor in order to decrease thermal losses and minimize temperature gradients at sample scale in the High-Temperature Chamber—HTC. The whole assembly lies upon thermal fins 6) for heat dissipation and, finally, on the global support 7). The experiments are carried out within the water-cooled confinement vessel 14) in an inert atmosphere of argon, in slight overpressure. The bichromatic video pyrometer 13) and the camera 14) allow for droplet imaging through adequate windows 10) and holes designed in the HTC. Finally, the whole acquisition data are collected by the data bus 15) and sent to the data acquisition computer 16), in parallel to the imaging computer 17), for sample monitoring 18).

2.1.2 Experimental Procedure, Measurement Principle, and Uncertainties

The original samples consist of specifically machined cylindrical pellets, whose both typical diameter and height are around 5 mm. Then, samples are mechanically polished, exposed to a chemical attack, and stored in acetone to avoid adverse oxidation prior to experimental tests. The average chemical compositions of the two studied alloys are measured before (as received) and after VITI-SD measurements (as tested). Spark spectrometers are used for general analysis of chemical composition by ICP-AES. Carbon, oxygen, sulfur, and nitrogen are measured with elementary combustion analyzers. Then, the initial atmosphere in the VITI confinement vessel is removed after several vacuum pumping/argon cleaning and monitored with a dedicated oximeter prior to the test. The induction heating is then started, and the sample is gradually heated with a 50°C/min temperature ramp until it reaches a liquid state, typically after a few dozen minutes (**Figure 2**).

At a given temperature of the aforementioned liquidus, the imaging system allows to take high-resolution pictures of the sessile droplet, as shown **Erreur ! Source du renvoi introuvable.** The sample is weighed before and after the test to ensure its mass m remains constant. By means of classical contour fitting techniques (Hoorfar, and Neumann, 2006), the droplet volume V can be determined, and thus density can be easily estimated: by definition, $\rho = m/V$. Then, other temperatures can be investigated to determine $\rho(T)$, up to the threshold of significant evaporation, and if required, beyond this threshold by extrapolation.

The sources of systematic uncertainty for density measurements at high temperatures are scaling uncertainty—linked to the resolution of the imaging system—leading to an error in volume estimation and temperature uncertainty. Mass uncertainty is negligible, given the weighing accuracy. Following JCGM 100 (2008), and according to Delacroix, et al. (2022), the relative systematic uncertainty associated with VITI-SD density measurements is about 1% when the experimental setup is carefully prepared.

2.1.3 Experimental Results

The measurements corresponding to six experimental tests are shown in **Figure 3**. The results clearly indicate a linear decrease of density with temperature following a linear tendency, as expected. There is no significant difference between 304LP1 and 304LP4 grades, which are almost identical in composition (except in minor elements). The density of ferritic steel 16MND5 is slightly higher than that of austenitic steel, given the larger iron content. The reproducibility between different samples is quite satisfying within experimental uncertainty. Additional details—such as original correlations $\rho(T)$—can be found in Chikhi, et al. (2019); Korobeinikov, et al. (2021); Delacroix, et al. (2022), in the framework of welding pool modeling.

2.2 VITI-MBP Configuration and Surface Tension Measurements

2.2.1 Experimental Layout

The VITI-MBP general layout is shown in **Figure 4**. Let us only introduce the main differences with VITI-SD. Here, the sample consists of a liquid steel pool 1) placed in a crucible 2). A zirconia-made capillary tube 3) of radius r is placed above the crucible and connected with the micrometer translation stage 12), which allows for the control of capillary immersion depth h into the liquid pool. A flow meter 13) regulates the argon gas flow in the capillary at a low gas flow rate. A pressure sensor 14) finally enables the measurement of pressure difference p between the capillary tip immersed in the pool and the surrounding atmosphere.

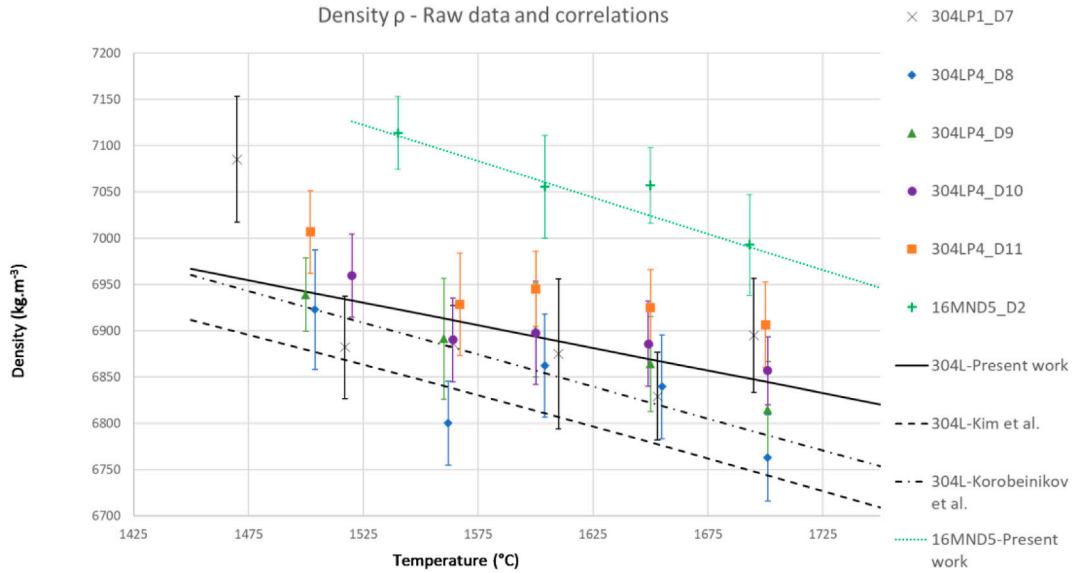

FIGURE 3 | VITI-SD density measurements and comparison with literature for 304L (Korobeinikov, et al., 2021; Kim, 1975).

2.2.2 Experimental Procedure, Measurement Principle, and Uncertainties

The experimental procedure for MBP tests is similar to the procedure for SD tests. The difference is that for MBP tests, slices of raw steel rods are directly used, constituting cylindrical loads whose typical diameter and height are around 30 and 45 mm, respectively. After atmosphere preparation and starting of induction heating, once the melting point is reached, the sample melts into a liquid pool, into which the capillary tube is immersed. The latter is carefully machined with high mechanical accuracy to allow for controlled bubbling inside liquid corium. The tip of the capillary tube is accurately controlled by means of a dedicated optical test bench: the surface roughness is assessed, and its inner diameter is determined with 10 µm accuracy, by edge detection after optical calibration.

As detailed in Dubberstein and Heller, (2013), at a given immersion depth h, typical pressure oscillations p are shown in the left-hand part of **Figure 5**. At the very beginning of the bubble growth process, the curvature radius r_b of the new bubble is much larger than the capillary radius: $r_b \gg r$. Consequently, a local pressure minimum is observed, representative from the hydrostatic pressure inside the pool. Then, the gas bubble begins to grow at the tip of the capillary tube. The pressure continuously grows up to a local maximum, for which $r = r_b$, corresponding to a growth duration t_{life}. At this local maximum, it is thus possible to derive the Laplace–Young equation as follows:

$$p = \frac{2\sigma}{r} + \rho g h,$$

thus giving access to surface tension σ, provided density ρ is known. Afterward, further immersion of the capillary tube into the molten pool allows achieving satisfying statistics, prior to the investigation of other temperatures. The quality of measurement results in a linear dependence $p(h)$, as shown in the right-hand part of **Figure 5**.

According to the Young–Laplace equilibrium, the main sources of systematic uncertainty for surface tension measurements at different temperatures are linked to geometry—capillary radius r and immersion depth h, pressure p, density ρ, and temperature T. Once again, following JCGM 100 (2008), and according to Delacroix, et al. (2022), the relative systematic uncertainty associated with VITI-MBP surface tension measurements is about 2.5%.

2.2.3 Experimental Results

The results corresponding to six experimental tests are reviewed in **Figure 6**. They tend to indicate that the surface tension of all vessel steel grades under consideration follow a concave parabolic evolution as a function of temperature. However, the peak of the parabola differs between grades with low sulfur content [S]—304LP1 and 16MND5—and the grade with high [S], namely, 304LP4. Moreover, the surface tensions of the three studied steels are ordered as follows: $\sigma_{304LP4} < \sigma_{304LP1} < \sigma_{16MND5}$.

Elemental analyses—that are not detailed here—confirm the impact of impurities. Recent articles (Korobeinikov, et al., 2021; Delacroix, et al., 2022) highlight the decisive role played by both sulfur and oxygen, acting similarly to surface active agents or surfactants. They tend to favor the decrease of surface tension values and may also influence the sign of $d\sigma/dT$ at a given temperature T. Additional details—such as original correlations $\sigma(T)$-- can be found in Korobeinikov, et al., (2021); Delacroix, et al., (2022) as well.

2.3 Discussion About the Influence on In-Vessel Corium Stratification and the Particular Issue of Focusing Effect

As previously mentioned, the IVR strategy is a mitigation strategy where corium is to be retained in the vessel by ex-vessel reactor vessel cooling by water to avoid vessel-wall melt-through. The

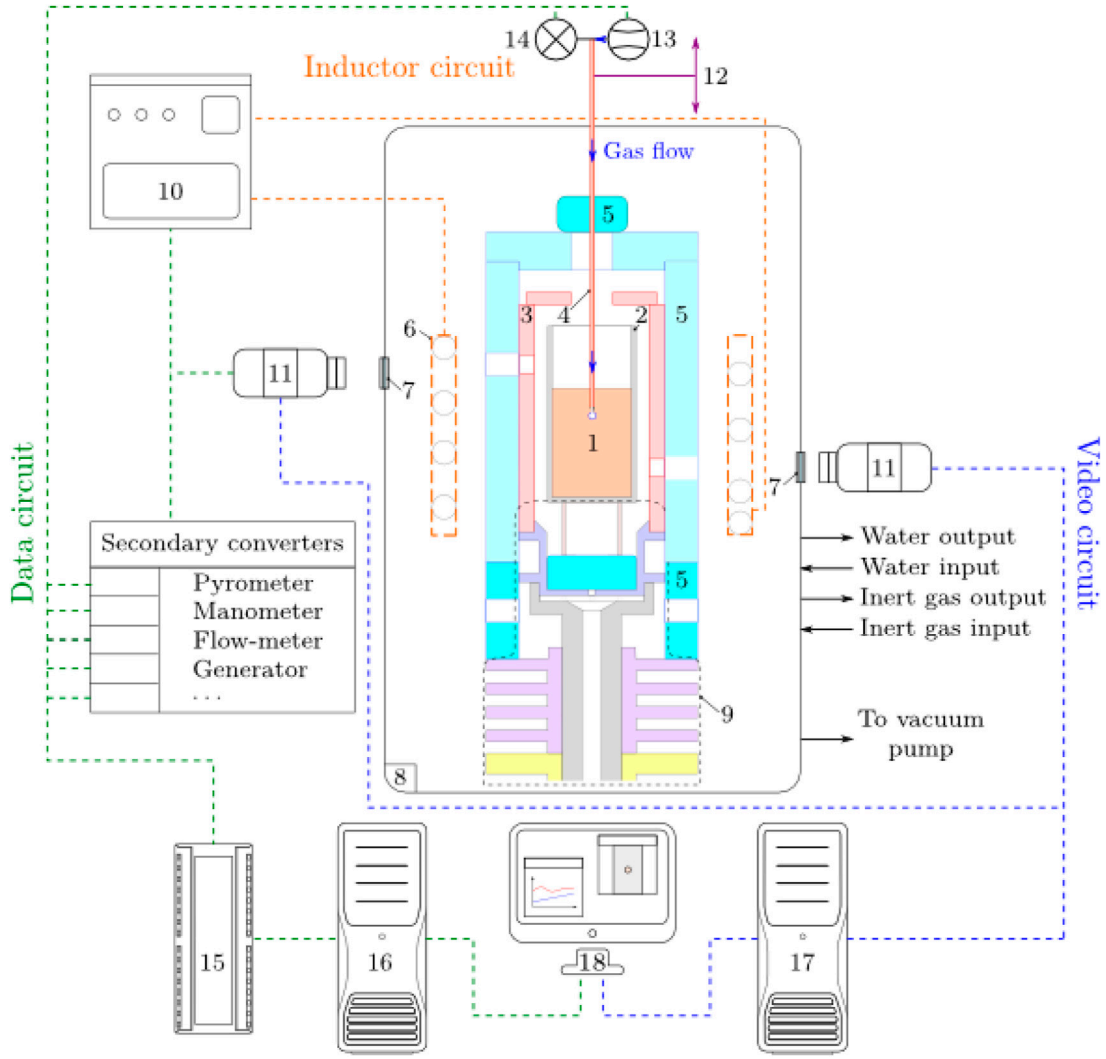

FIGURE 4 | Overall layout of VITI-MBP configuration (Delacroix, et al., 2022). 1: liquid pool; 2: crucible; 3: susceptor support; 4: capillary tube; 5: thermal shield; 6: inductor; 7: windows; 8: confinement vessel; 9: supporting system; 10: generator; 11: pyrometers; 12: µm translation stage; 13: µ-flow meter; 14: µ-pressure sensor; 15: data bus; 16: acquisition PC; 17: imaging PC; 18: monitoring.

success of the strategy mainly depends on the heat flux distribution at the corium pool interface compared to the Critical Heat Flux (CHF), above which vessel integrity is not ensured.

As shown on the left part of **Figure 7**, the corium pool configuration is rather complex, in link with the existence of miscibility gaps between the oxide (*e.g.*, UO_2-ZrO_2) and the metallic (*e.g.* light: steel—mainly Fe; heavy: Zr-U) phases. Three main areas may be roughly distinguished: the molten oxide pool, possibly surrounded by a solid crust; the heavy metal layer, at the very bottom of the vessel; and the light metal layer, on top of the oxide pool.

The presence of this thin upper metallic layer is a major issue. The heat produced by the decay of fission products in the oxide pool can be preferentially transferred to the upper metallic layer, which in turn transfers it to the vessel wall. Assuming high thermal conductivity of liquid metal compared to the oxide pool, the main part of the thermal load on the vessel may be concentrated in the metallic layer, leading to the so-called "focusing effect" phenomenon.

Historically, stationary IVR studies have been performed to quantify the thermal load from the molten pool to the vessel wall (Rempe, et al., 1997; Esmaili and Khatib-Rahbar, 2005; Theofanous, et al., 1997). More recently, a transient approach to the stratified corium pool (Seiler, et al., 2007; Zhang, et al., 2011; Le Tellier, et al., 2015) and a benchmark between different severe accident scenario codes (Sangiorgi, 2015) pointed out that the use of conservative assumptions may result in heat fluxes exceeding the CHF, in link with the focusing effect. If now, we focus on the thermal-hydraulics of the upper metallic layer, recent Computational Fluid Dynamics (CFD) simulations showed that bulk convection is mainly driven by the Rayleigh–Bénard instability and lateral recirculation along the cooled vessel wall

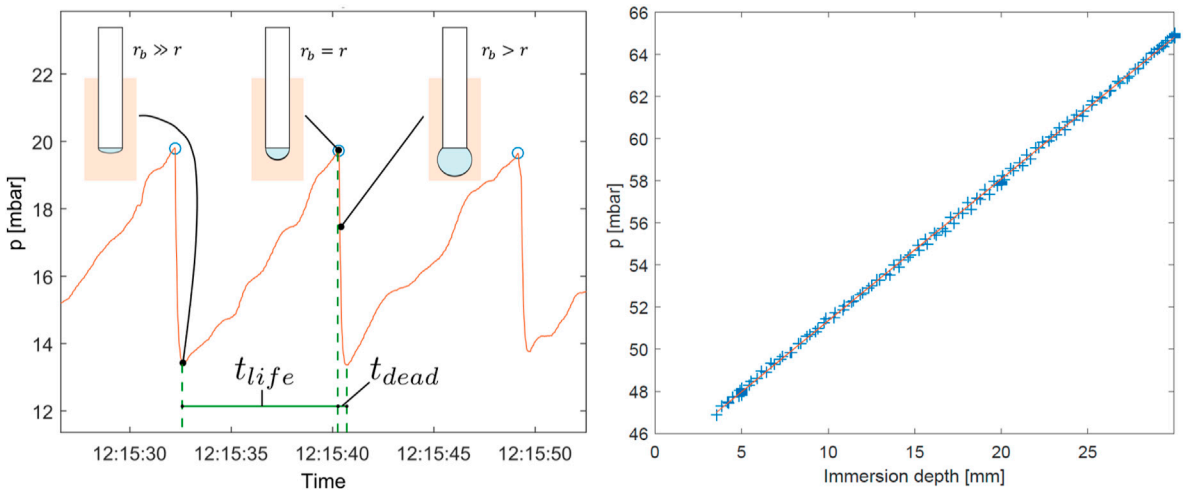

FIGURE 5 | Principle of VITI-MBP measurements at given temperature T. Left: pressure p peak detection at given immersion depth h. Right: linear correlation $p(h)$.

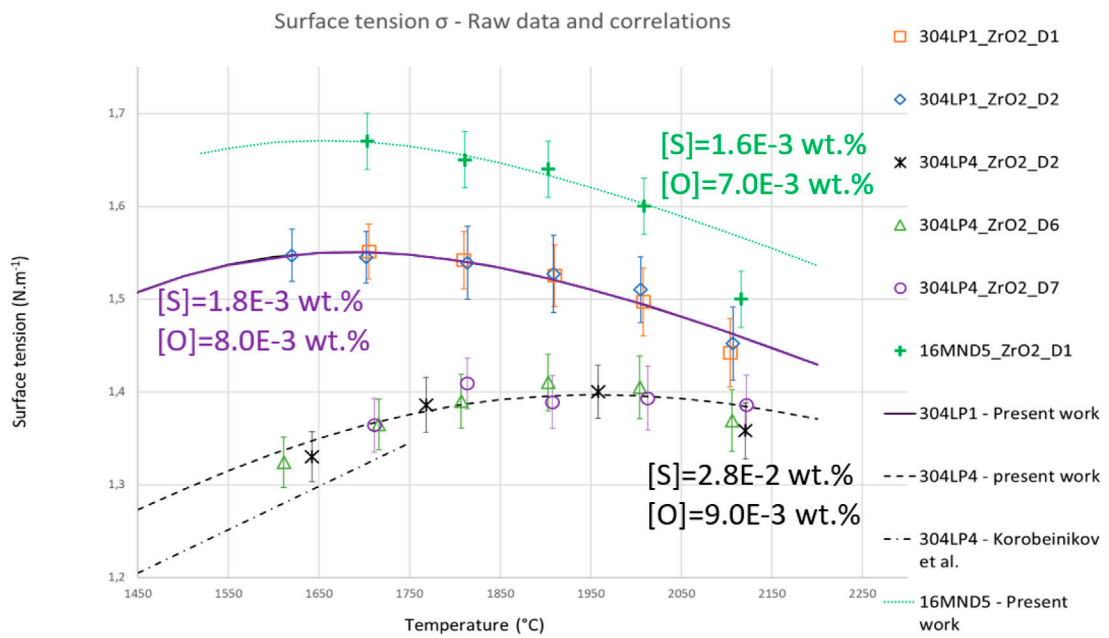

FIGURE 6 | VITI-MBP surface tension measurements and comparison with literature at "low" temperatures for 304L (Korobeinikov, et al., 2021; Delacroix, et al., 2022). The mass fraction of sulfur [S] and oxygen [O] related to each grade is also indicated.

(Saas, et al., 2017), for which the evolution of density ρ with temperature T plays a significant role, along with viscosity as well. For thin enough metallic layers, the Bénard–Marangoni effect may also significantly influence the flow topology. As shown in **Figure 7**(right), depending on the dependence of surface tension σ on temperature, the surface flow could either promote or impede the Rayleigh–Bénard convection. In particular, if σ decreases with T, the co-current surface and bulk flows will favor heat extraction at the free surface, thus reducing the thermal load on the vessel wall (Dang, et al., 2021).

Concerning density, the measurements performed with VITI-SD shown in **Figure 3** can be directly used to feed CFD simulations of the Rayleigh–Bénard convection patterns governing the thermal-hydraulics of the upper metallic layer. The linear decrease with temperature confirms the predicted orientation of Rayleigh–Bénard cells, with a slight difference in magnitude expected between the different steel grades according to the change in temperature coefficients.

Concerning surface tension, in the light of the results shown in **Figure 6**, the level of surface tension at the free surface of the top

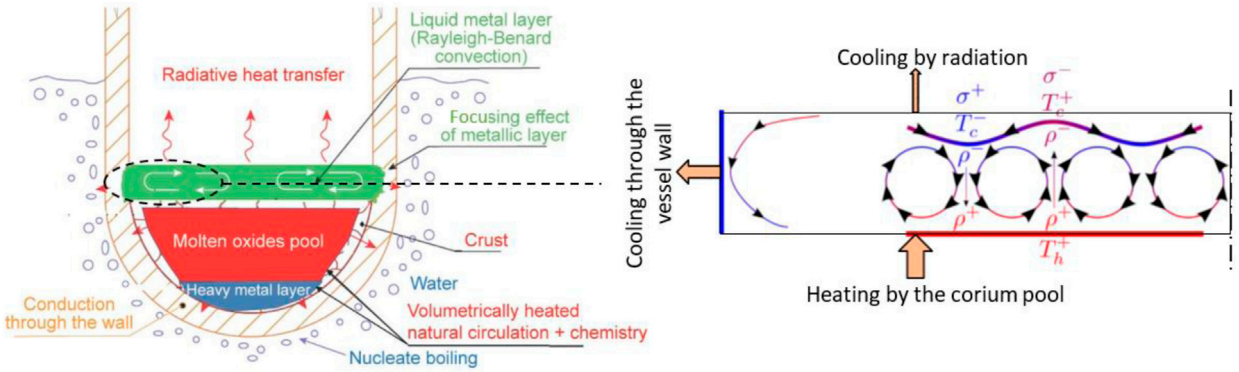

FIGURE 7 | Typical IVR configuration. Left: stratified corium pool and typical transfer phenomena (Ma, et al., 2016). Right: zoom on the Bénard-Marangoni flow at the surface of the thin upper metallic layer, according to surface tension evolution with temperature (courtesy from R. Le Tellier).

metallic layer may significantly vary according to local composition. As the Bénard–Marangoni surface flow directly depends on the temperature coefficient of surface tension $d\sigma/dT$, the surface flow could alternatively promote or impede the Rayleigh–Bénard convection depending on temperature range and actual melt composition. This means that whether in transient regime and/or if the free surface experiences significant thermal (and/or compositional) gradients, the resulting inflection in the surface tension profile could lead to complicated flow topologies in the metallic layer stemming from local surface tension gradient. This amends the conclusion of Chikhi, et al. (2019) to some extent, where the case $d\sigma/dT > 0$ seemed the most probable considering preliminary results.

3 MEASURING THE SOLIDUS/LIQUIDUS TEMPERATURES AND THE VISCOSITY OF LIQUID OXIDES AT HIGH TEMPERATURES FOR EX-VESSEL RETENTION: THE VITI-VPA AND VITI-GFL CONFIGURATION

Let us now turn to the investigation corium spreading in link with the EVR strategy. In this case, the VITI facility is used to gain physical insight about ex-vessel corium phase transitions and rheology, especially for oxides in the present article. On the one hand, the Visual Polythermal Analysis—VPA—technique is used for the measurement of solidus and liquidus temperatures T_{sol} and T_{liq}, respectively. On the other hand, the Gas Film Levitation—GFL—technique is implemented to give a first estimate of dynamic viscosity η.

3.1 VITI-VPA Configuration and Solidus/Liquidus Temperatures

3.1.1 Experimental Layout

The VITI-VPA general layout is shown in **Figure 8**. The single difference with VITI-SD configuration is the supporting system, which defines a field-of-view more convenient for phase transition detections by the camera focusing on the (originally) solid corium pellet.

3.1.2 Experimental Procedure, Measurement Principle, and Uncertainties

The experimental procedure for VPA tests is exactly the same as for SD tests, except that the solid oxide pellets of corium are specifically machined in a glove box before transferring them into the VITI confinement vessel in controlled conditions. Before reaching high temperatures, the pellets are subjected to heat treatment for a dozen minutes far below theoretical solidus (around 500°C) to eliminate residual organic pollution. Once melted, both high-definition (HD) camera and video-pyrometers constitute the polythermal imaging system for the VITI-SD tests, whose typical configuration is shown in **Figure 9**. Video-pyrometer 1 focuses on the top of the melting sample, thus measuring the temperature T_{sample}, while video-pyrometer 2 focuses on the substrate, thus giving the temperature $T_{substrate}$. The HD camera allows for sharp imaging of the substrate/sample system.

The methodology applied for VITI-VPA experiments derived from the approach proposed in Bechta (2007) is depicted in **Figure 10**. The high-resolution camera allows for a visual online detection of both solidus and liquidus points, in correlation with temperature measurements, by scrutinizing the first—respectively last—evidence of a liquid—respectively solid—phase at the surface of the sample. This allows us to define a first "solidus interval" $[T^-_{sol,vid}, T^+_{sol,vid}]$ – respectively "liquidus interval" $[T^-_{liq,vid}, T^+_{liq,vid}]$ – based on imaging interpretation.

In parallel, the posttreatment of temperature data supplied by the pyrometers alone, or polythermal analysis, is used as a complementary measurement procedure. The quantity corresponding to the temperature difference $\Delta T = T_{sample} - T_{substrate}$ can be defined from video-pyrometers alone. As shown in **Figure 10**, close to both solidus and liquidus temperatures, the evolution of ΔT shows noticeable inflection points due to swift changes of surface radiative properties and the enthalpy difference caused by phase transition. This polythermal

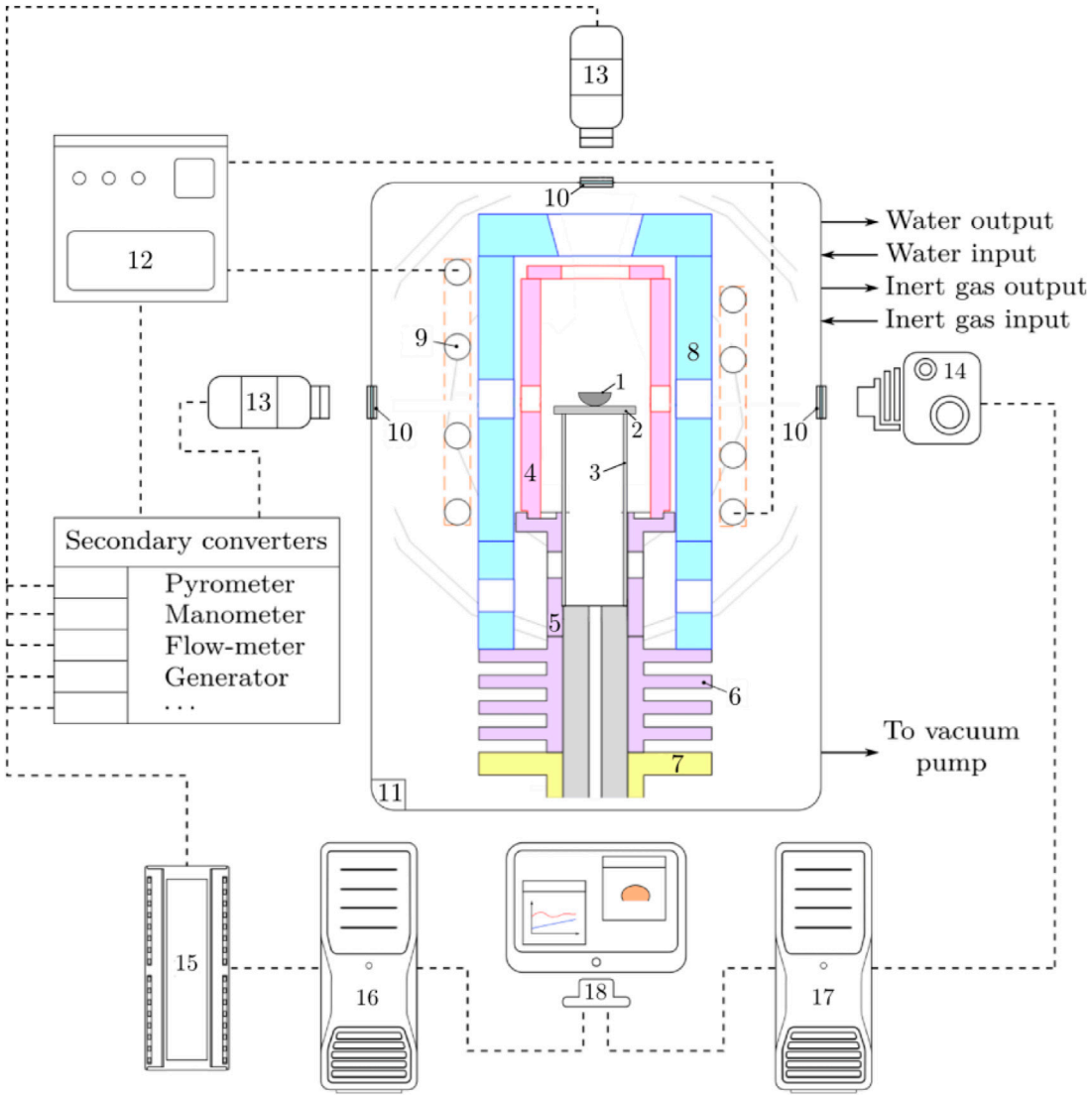

FIGURE 8 | Overall layout of VITI-VPA configuration (Delacroix, et al., 2019). 1: corium sample; 2: substrate; 3: substrate support; 4: susceptor; 5: susceptor support; 6: fins; 7: global support; 8: thermal shield; 9: inductor; 10: windows; 11: confinement vessel; 12: generator; 13: pyrometers; 14: camera; 15: data bus; 16: acquisition PC; 17: imaging PC; 18: monitoring.

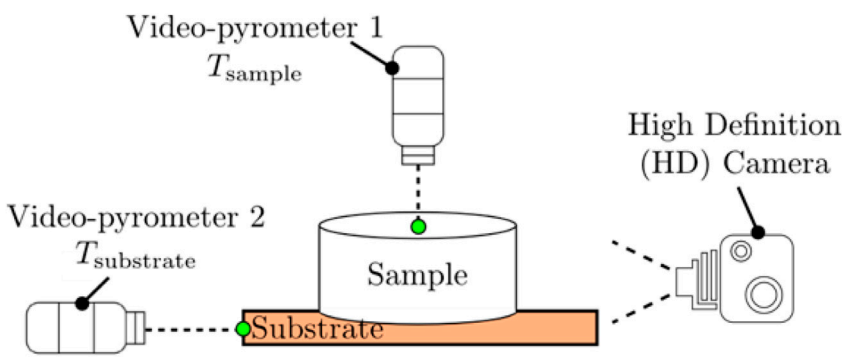

FIGURE 9 | Visual Polythermal Analysis (VPA) imaging system of VITI.

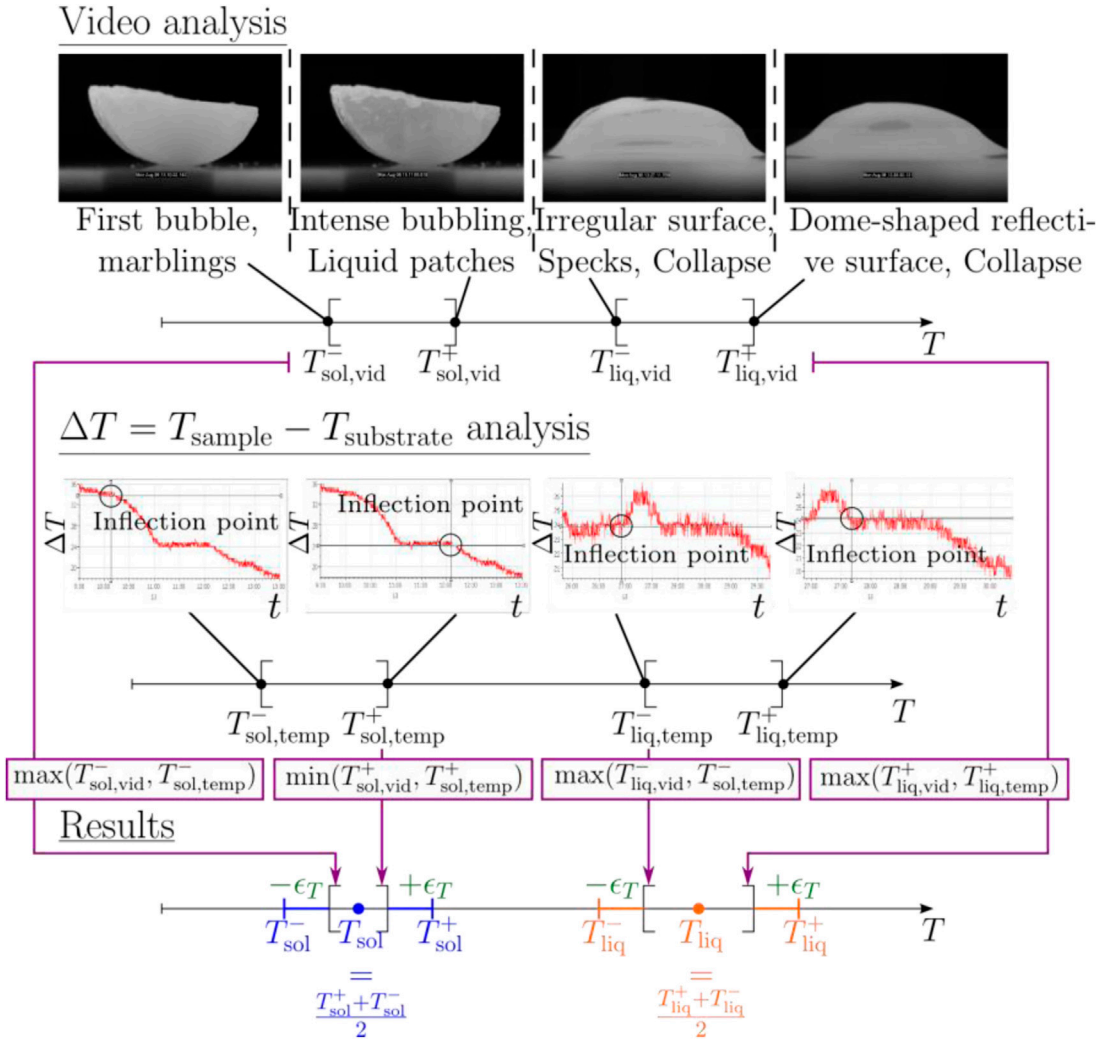

FIGURE 10 | Principle of visual polythermal analysis.

analysis leads to the definition of other temperature intervals, both for solidus $[T^-_{\mathrm{sol,temp}}, T^+_{\mathrm{sol,temp}}]$ and liquidus $[T^-_{\mathrm{liq,temp}}, T^+_{\mathrm{liq,temp}}]$.

The two approaches are then merged through VPA, leading to the definition of best-estimated intervals for both T_{sol} and T_{liq}. The main sources of systematic uncertainty for solidus/liquidus measurements are obviously linked to camera resolution for visual detection and to pyrometer accuracy. According to Delacroix, et al. (2019), the relative systematic uncertainty associated with VITI-VPA solidus and liquidus temperature measurements amounts typically to 3%.

3.1.3 Experimental Results

Let us give an application in link with corium spreading by discussing the results originally presented in Delacroix, et al. (2019) and shown **Figure 11**. The solidus and liquidus temperatures of various CSM mixtures (confidential composition) are measured according to the mass fraction of the corium. Obviously, the addition of sacrificial material to corium significantly lowers liquidus temperatures and solidus temperatures to a lesser extent. The reader may find additional details in Delacroix, et al. (2019), including comparisons with thermodynamic calculations.

3.2 VITI-GFL Configuration and Viscosity Measurements

3.2.1 Experimental Layout

The VITI-GFL general layout is shown in **Figure 12**. Let us only introduce the main differences with VITI-SD. Here, the liquid drop 1) is levitated on the lower diffuser 2) made of porous graphite, avoiding contact with the substrate by means of a thin gas film. The upper diffuser 5) can be vertically translated and constitutes the mobile actuator enabling droplet

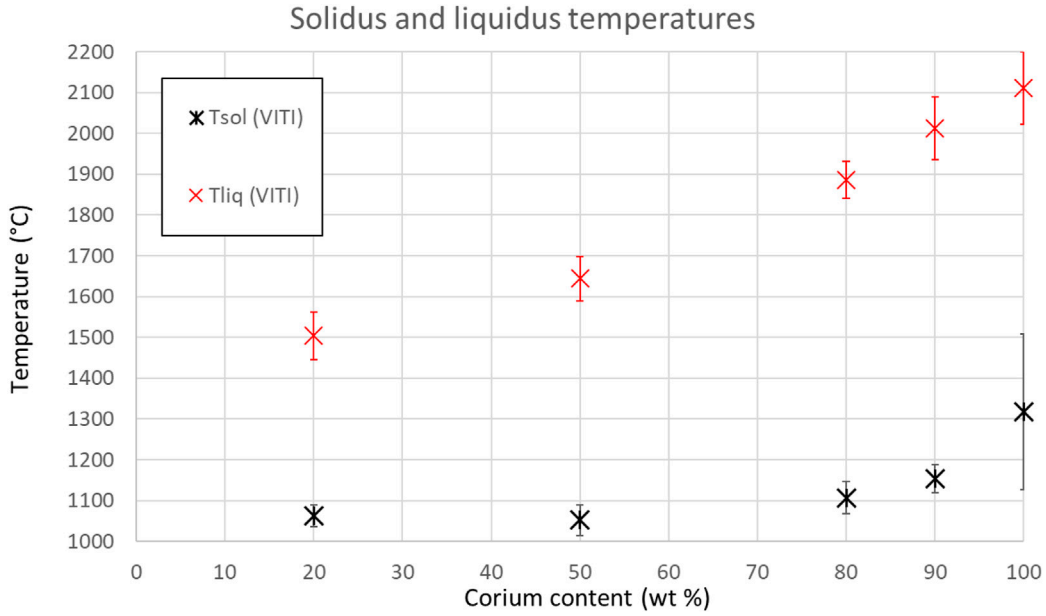

FIGURE 11 | VITI-VPA solidus and liquidus temperature measurements, according to corium content in Corium-Sacrificial Material (CSM) mixtures (Delacroix, et al., 2019).

relaxation for measuring dynamic viscosity η. This configuration minimizes the potential chemical interaction between the melt and its environment (substrate or crucible in other configurations).

3.2.2 Experimental Procedure, Measurements Principle, and Uncertainties

The experimental procedure for GFL tests is almost the same as for SD tests. The main challenge is to ensure the correct levitation of the sample, which is specifically machined to assess its stability at a solid state over the thin gas film and when moving the upper actuator before heating.

The principle of VITI-GFL measurement is based on the analysis of droplet relaxation. As shown in **Figure 13**, the liquid droplet is initially "at rest", levitating on the thin gas film generated by the lower diffuser. Then, the upper diffuser is drawn closer to the droplet. Once again, a thin gas film avoids any direct contact between the droplet and the diffuser. The upper diffuser is translated further downward so that the liquid droplet apex is subjected to an initial slight deformation of Δh_0 from its initial position h_0. The upper diffuser is then instantly moved upward, and the droplet experiences free oscillations. The time-evolution of droplet apex position h is tracked by means of a high-speed camera.

Droplet oscillations are governed by the values of the Ohnesorge number, defined by $\mathrm{Oh} = \eta/\sqrt{\sigma\rho R_S}$, where R_S is the radius of the equivalent sphere with the same volume as the liquid droplet. If $\mathrm{Oh} > 1$, the aperiodic mode prevails, while if $\mathrm{Oh} < 1$, the pseudo-periodic mode prevails—see **Figure 13**.

In this article, let us only focus on the pseudo-periodic mode. In this case, the time evolution of droplet apex position h can be written as follows:

$$h(t) = h_0 + \Delta h_0 \exp\left(-\frac{t}{\tau_p}\right)\cos(\omega t + \varphi),$$

where τ_p, ω, and φ correspond to damping time, angular frequency, and phase. In practice, this equation is fitted on the experimental profile. The fitted parameter of interest is τ_p because it can be linked to viscosity owing to a variational approach based on the analogy with damped mechanical harmonic oscillators (Haumesser, et al., 2002) deriving from Chandrasekhar formalism (Chandrasekhar, 1970). In fact, $\tau_p = f(\text{geometry}, \rho, \sigma, \eta)$. Density and surface tension being determined apart, for example, by VITI-SD and VITI-MBP experiments, it is thus possible to estimate the dynamic viscosity of the liquid sample.

As for VITI-SD, the main sources of systematic uncertainty for viscosity measurements at high temperatures are scaling uncertainty—linked to the resolution of the imaging system—leading to an error in apex location detection limit and temperature uncertainty. According to Grishchenko and Piluso (2011), the relative systematic uncertainty associated with VITI-GFL density measurements can amount to 10%; given the difficulty to properly track the exact position of the droplet apex, the magnitude of the initial deformation being restricted in order to apply the model based on the underlying linear perturbation theory.

3.2.3 Experimental Results

An application of VITI-GFL measurements is given in **Figure 14**, where prospective results are obtained for pure alumina Al_2O_3 and for the zirconia–alumina eutectic composition ZrO_2 (42.5 wt%)-Al_2O_3. First, the addition of zirconia to alumina at eutectic composition allows decreasing

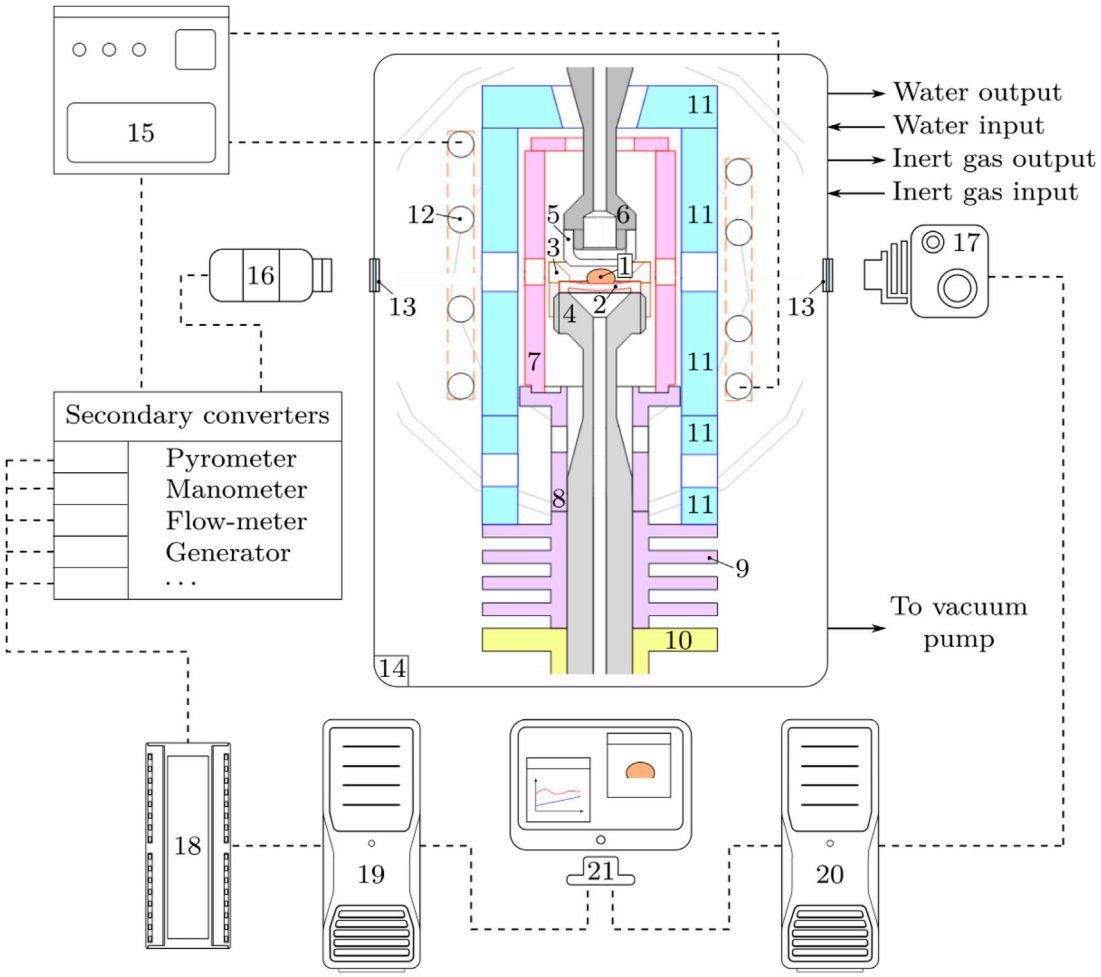

FIGURE 12 | Overall layout of VITI-GFL configuration (Grishchenko and Piluso, 2011). 1: drop; 2: lower diffuser; 3: screwing system; 4: lower diffuser holder; 5: upper diffuser; 6: upper diffuser holder; 7: susceptor; 8: susceptor holder; 9: fins; 10: global support; 11: thermal shield; 12: inductor; 13: windows; 14: VITI confinement vessel; 15: generator; 16: pyrometer; 17: high-speed camera; 18: data bus; 19: data acquisition computer; 20: imaging computer; 21: monitoring.

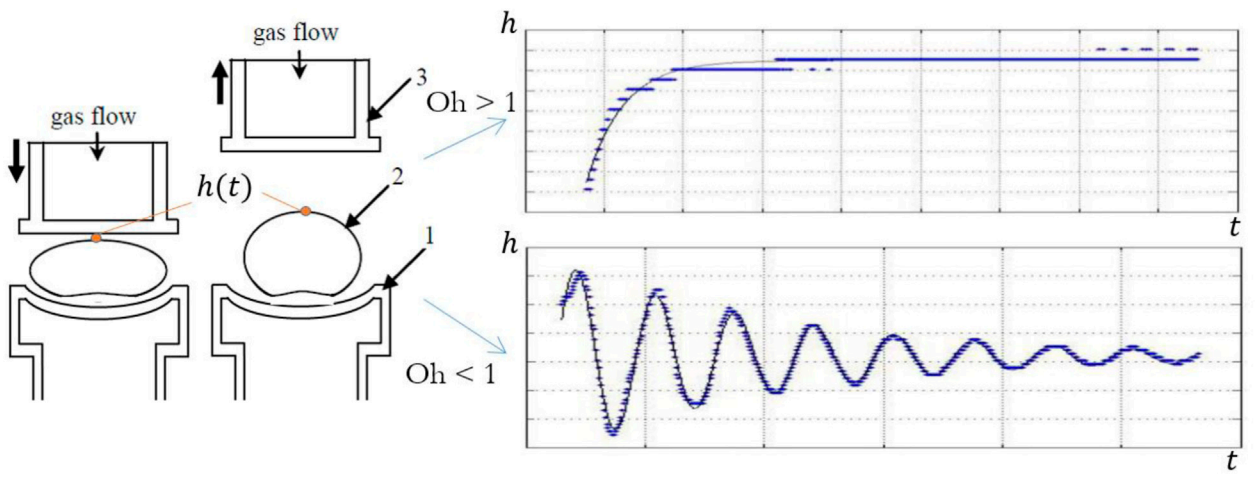

FIGURE 13 | Estimation of dynamic viscosity by droplet apex tracking with VITI-GFL.

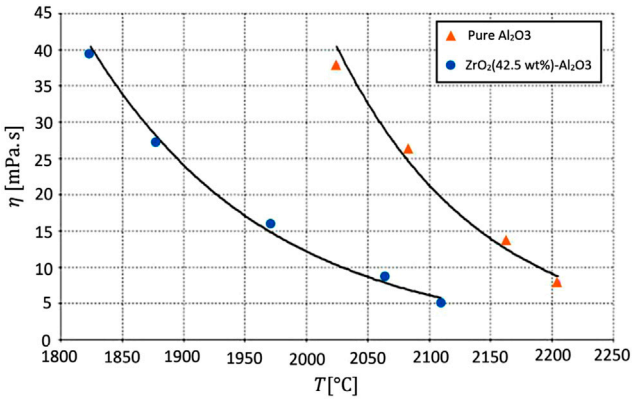

FIGURE 14 | VITI-GFL viscosity measurements of alumina and zirconia-alumina eutectic, from Grishchenko and Piluso (2011).

the liquidus temperature—from 2025°C to 1825°. Then, the viscosity of pure alumina is found significantly larger than the viscosity of the eutectic composition at a given temperature for which both are at liquid state.

3.3 Discussion About the Influence on Ex-Vessel Retention Strategy and the Particular Issue of Corium Spreading

In the EVR strategy, the surface-to-volume ratio of corium must be maximized to increase coolability. In the EPR core catcher concept (Fischer, et al., 2016), and as a backfit for some Gen 2 reactors (Bonnet, et al., 2016), spreading is a means to reduce the melt thickness and thus the average heat fluxes to concrete, as shown **Figure 15**. Spreading is, indeed, controlled by the melt properties, mainly kinematic viscosity (Journeau, et al., 2003). For additional safety improvements in both central and lateral approaches, sacrificial materials can be used to improve molten core coolability by effectively spreading the molten core on the concrete basemat to form a thin layer. The addition of such sacrificial materials into the melt aims, indeed, at lowering the viscosity of the resulting Corium-Sacrificial Material (CSM) mixture and lowering its liquidus temperature compared to that of mere corium. The influence of liquidus (and solidus) temperatures—related to phase transitions—and viscosity and their measurements are also discussed in this article.

As shown in **Figure 11**, the VITI-VPA measurements clearly demonstrate that the addition of judicious sacrificial material to corium significantly lowers liquidus temperatures. The decrease of liquidus temperature obviously promotes corium spreading: the longer corium remains at a liquid state, the further it will spread. At the reactor scale, this validates the choice of the sacrificial material under consideration as it will be gradually incorporated into the melt while interacting with corium, thus delaying its freezing and favoring spreading.

Now, concerning viscosity, and by analogy with the CSM issue, considering in **Figure 14** that alumina stands for corium and zirconia for sacrificial material, one could conclude that the addition of relevant materials into the melt may not only succeed in altering phase transitions but may also deeply influence corium rheology. A first simplified approach could assume the following statement: if dynamic viscosity follows the same trend as solidus/liquidus temperatures, then it is a two-fold positive effect for corium spreading. If not, then a competition shall occur between the thermodynamic and thermophysical properties.

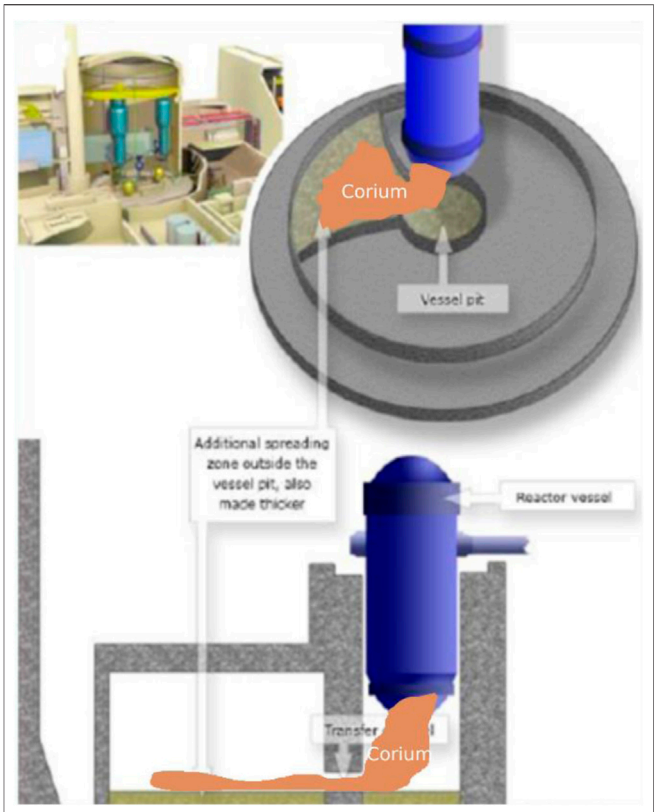

FIGURE 15 | Ex-Vessel Retention Strategy and corium spreading over a large surface, as adapted from Bonnet, et al. (2016).

4 CONCLUSION

Within the framework of corium characterization at high temperatures, a consistent approach has been proposed in the present article in order to fill the lack of such fundamental data as density, surface tension, liquidus and solidus temperatures, and viscosity. The discussion highlights the prominent role played by such properties in the physical mechanisms governing the behavior of corium, when applied to In-Vessel Retention—IVR—and Ex-Vessel Retention—EVR—strategies. Concerning the IVR mitigation strategy, in link with the focusing effect issue at the thin upper metallic layer, the influence of density and surface tension has been discussed. Concerning the EVR mitigation strategy, the impact of solidus/liquidus temperatures and dynamic viscosity on corium spreading has been pointed out

for oxide samples. The unique capacities of the VITI facility have been highlighted: indeed, VITI has been declined into various configurations, enabling access to the original experimental measurements for the properties of interest at high temperatures.

The different configurations of the VITI facility can be applied to a variety of oxide and metallic corium compositions representative of nuclear reactor severe accidents. For instance, if in the present article only metallic compositions are discussed for the VITI-MBP experimental setup, the MBP technique has also been applied to oxide corium compositions, giving access to original data for both in-vessel (Chikhi, et al., 2021) and ex-vessel (Delacroix, et al., 2020) corium compositions.

Corium thermophysical property measurements at high temperatures constitute an experimental issue that is now addressed by the VITI facility through its different configurations. The potential high variability of such properties with temperature prevents from adopting a classical parametric approach as far as numerical simulations are concerned. For instance, the viscosity may vary by several orders of magnitude, depending on the working temperature, especially considering the large solidification intervals often associated with such multicomponent systems as corium. It is most likely that large parts of the domain (composition, temperature, and pressure) shall remain inaccessible to the experimental approach. A relevant example is found when considering the stratified corium pool in the IVR strategy: the liquid/liquid interfacial tension between the oxide layer and the metallic layer may be required to compute corium pool thermal hydraulics (Zanella, et al., 2021), but the MBP approach gives only access to liquid/gas surface tensions. As proposed, for example, in Gajavalli and Le Tellier (2022), a modeling approach allowing to deduce liquid/liquid interfacial tension from separate surface tension measurements could provide further physical insight into corium pool topology.

In order to enhance severe accident code simulation reliability for various nuclear reactor types (PWRs, BWRs, and CANDU), reliable corium properties both in composition and in temperature are absolutely needed. Acquiring experimental thermophysical property data on key properties and corium compositions should be the first step. The general modeling of thermophysical properties should be the second step. The final step would be the building of thermophysical property databases coupled with severe accident codes. Such kind of approach is under construction in the frame of national and international projects.

DATA AVAILABILITY STATEMENT

The data analyzed in this study is subject to the following licenses/restrictions: Restricted access due to organization policy. Requests to access these datasets should be directed to the corresponding author.

AUTHOR CONTRIBUTIONS

JD, CJ, and PP carried out the experiments and related analytical work and wrote this article in a collegial manner.

ACKNOWLEDGMENTS

The authors would like to express their special thanks to Dr. Romain Le Tellier for many insightful discussions and to Dr. Christophe Suteau for his constant support.

REFERENCES

Amidu, M. A., Olatubosun, S. A., Ayodeji, A., and Addad, Y. (2022). Severe Accident in High-Power Light Water Reactors: Mitigating Strategies, Assessment Methods and Research Opportunities. *Prog. Nucl. Energy* 143, 104062. - ISSN: 0149-1970. doi:10.1016/j.pnucene.2021.104062

Asmolov, V., and Tsurikov, D. (2000). "RASPLAV Project : Major Activities and Results [Conference]," in Proceeding of the OECD/NEA RASPLAV Seminar, Munich, Germany.

Baek, W.-P., Yang, J.-E., Ball, J., Glown, G., Bisconti, G., Peko, D., et al. (2017). Safety Research Opportunities Post-Fukushima. Initial Report of the Senior Expert Group. Boulogne-Billancourt: Organisation for Economic Co-Operation and Development, NEA-OECD.

Bakuta, N., Le Tellier, R., and Saas, L. (2015). "Assessment of Advanced Corium-In-Lower-Head Models in MAAP and PROCOR Codes," in Proc. ERMSAR 2015, 7th Eur. Rev. Mtg. Sev. Acc. Res., Marseille, France. [Conference].

Bechta, S. V., Krushinov, E. V., Almjashev, V. I., Vitol, S. A., Mezentseva, L. P., Petrov, Y. B., et al. (2007). Phase Diagram of the UO2-FeO1+x System. *J. Nucl. Mater.* 362, 46–52. - ISSN: 0022-3115. doi:10.1016/j.jnucmat.2006.11.004

Bonnet, J. M., Robledo, F., Farmer, M. T., Cranga, M., Spengler, C., Vola, D., et al. (2017). State of the Art Report on Molten Core Concrete Interaction and Ex-Vessel Molten Core Coolability, NEA-OECD.

Bonnet, J. M., Raimond, E., Cenerino, G., Vola, D., and Fichot, F. (2016). "Strategy for the Corium Stabilisation in Case of a Severe Accident for the French PWRs," in IAEA Technical Meeting on Phenomenology and Technologies Relevant to In-Vessel Melt Retention and Ex-Vessel Corium Cooling, Shanghai, China, October 2016. [Report] : Tech. rep.

Brooks, R. F., Dinsdale, A. T., and Quested, P. N. (2005). The Measurement of Viscosity of Alloys—A Review of Methods, Data and Models [Journal]. *Meas. Sci. Technol.* 16, 354–362. doi:10.1088/0957-0233/16/2/005

Carénini, L., Fichot, F., and Seignour, N. (2017). Modelling Issues Related to Molten Pool Behaviour in Case of In-Vessel Retention Strategy. *Ann. Nucl. Energy* 118, 363–374. doi:10.1016/j.anucene.2018.04.032

Chandrasekhar, S. (1970). *Hydrodynamic and Hydromagnetic Stability [Book]. - [s.l.]*. Dover publications.

Chikhi, N., Delacroix, J., Fouquart, P., and Turquais, B. (2021). Measurement of Corium Surface Tension Using the Maximum Bubble Pressure. *Nucl. Eng. Des.* 379, 111266. doi:10.1016/j.nucengdes.2021.111266

Chikhi, N., Fouquart, P., Delacroix, J., and Piluso, P. (2019). Measurement of Type 304L Stainless Steel and 16MND5 Ferritic Steel Density and Surface Tension: Possible Impact for Stratified Molten Pool. *Nucl. Technol.* 205, 200–212. doi:10.1080/00295450.2018.1486160

Dang, C., Peybernes, M., Le Tellier, R., and Saas, L. (2021). Numerical Simulations of the Rayleigh-Bénard-Marangoni Convections in a Thin Metallic Layer [Journal]. *Ann. Nucl. Energy* 150, 107848. doi:10.1016/j.anucene.2020.107848

Delacroix, J., Chikhi, N., Fouquart, P., Journeau, C., Tatsahura, K., Tsukamoto, T., et al. (2019). "Solidus and Liquidus Temperatures of Corium-Sacrificial

Material Mixtures: Experimental Results and Thermodynamic Calculations [Conference]," in Proceedings of FDR2019, International Topical Workshop on Fukushima Decommissioning Research.

Delacroix, J., Journeau, C., Chikhi, N., Fouquart, P., and Zhan, D. (2020). Measurements of In-Vessel and Ex-Vessel Liquid Corium Surface Tension and Density in the VITI-MBP Test Bench within ALISA Euro-Chinese Project. *Mech. Eng. J.* 7, 611. doi:10.1299/mej.19-00611

Delacroix, J., Piluso, P., Chikhi, N., Asserin, O., Borel, D., Brosse, A., et al. (2022). Measurements of Liquid AISI 304L Steel Density and Surface Tension, and Influence of Surface-Active Elements at High Temperatures. *Steel Res. Int.* 2100624. doi:10.1002/srin.202100624

Dubberstein, T., Heller, H.-P., Klostermann, J., Schwarze, R., and Brillo, J. (2015). Surface Tension and Density Data for Fe-Cr-Mo, Fe-Cr-Ni, and Fe-Cr-Mn-Ni Steels. *J. Mater Sci.* 11 0150, 7227–7237. doi:10.1007/s10853-015-9277-5

Dubberstein, T., and Heller, H.-P. (2013). The Thermophysical Properties of Liquid TRIP/TWIP-Steel Alloys Using the Maximum Bubble Pressure Method. *Adv. Eng. Mat.* 15, 583–589. doi:10.1002/adem.201200310

Egry, I., and Brillo, J. (2009). Surface Tension and Density of Liquid Metallic Alloys Measured by Electromagnetic Levitation. *J. Chem. Eng. Data* 54, 2347–2352. doi:10.1021/je900119n

Esmaili, H., and Khatib-Rahbar, M. (2005). Analysis of Likelihood of Lower Head Failure and Ex-Vessel Fuel Coolant Interaction Energetics for AP1000. *Nucl. Eng. Des.* 235, 1583–1605. doi:10.1016/j.nucengdes.2005.02.003

Farmer, M. T., Gerardi, C., Bremer, N., and Basu, S. (2016). Key Findings and Remaining Questions in the Areas of Core-Concrete Interaction and Debris Coolability. *Nucl. Technol.* 196, 10. doi:10.13182/nt16-43

Fichot, F., Carénini, L., Bakouta, N., Esmaili, H., Humphries, L., Laato, T., et al. (2020). Elaboration of a Phenomena Identification Ranking Table (PIRT) for the Modelling of In-Vessel Retention [Journal]. *Ann. Nucl. Energy* 146, 107617. doi:10.1016/j.anucene.2020.107617

Fichot, F., Michel, B., Almjashev, V., Le Guennic, C., Bakouta, N., Le Tellier, R., et al. (2022). Chemical Interactions of Molten Steel with (U-Zr-O) Corium: Main Outcomes of the CORDEB Program. *Nucl. Eng. Des.* 388, 111588. doi:10.1016/j.nucengdes.2021.111588

Fischer, M., Bechta, S. V., Bezlepkin, V. V., Hamazaki, R., and Miassoedov, A. (2016). Core Melt Stabilization Concepts for Existing and Future LWRs and Associated Research and Development Needs. *Nucl. Technol.* 196, 524–537. doi:10.13182/nt16-19

Fischer, M. (2004). The Severe Accident Mitigation Concept and the Design Measures for Core Melt Retention of the European Pressurized Reactor (EPR). *Nucl. Eng. Des.* 230, 169–180. - 11th International Conference on Nuclear Energy. - ISSN: 0029-5493. doi:10.1016/j.nucengdes.2003.11.034

Gajavalli, K., and Le Tellier, R. (2022). Butler-based Thermodynamic Modelling of Interfacial Energies for In-Vessel Corium Systems. *J. Nucl. Mater.*. (submitted).

Grishchenko, D., and Piluso, P. (2011). Recent Progress in the Gas-Film Levitation as a Method for Thermophysical Properties Measurements: Application to ZrO2-Al 2O3 System [Journal]. *High. Temperatures-High Press.* 40, 127–149.

Haumesser, P.-H., Bancillon, J., Daniel, M., Perez, M., and Garandet, J.-P. (2002). High-temperature Contactless Viscosity Measurements by the Gas-Film Levitation Technique: Application to Oxide and Metallic Glasses. *Rev. Sci. Instrum.* 73, 3275–3285. doi:10.1063/1.1499756

Hoorfar, M., and W. Neumann, A. (2006). Recent Progress in Axisymmetric Drop Shape Analysis (ADSA). *Adv. Colloid Interface Sci.* 121, 25–49. doi:10.1016/j.cis.2006.06.001

JCGM 100 (2008). *Evaluation of Measurement Data - Guide to the Expression of Uncertainty in Measurement [Report]*.

Journeau, C. (2006). *L'étalement du corium: Hydrodynamique, Rhéologie et Solidification d'un bain d'oxydes à hautes températures [Report]*. Ph.D. dissertation. France: University of Orléans.

Journeau, C., Boccaccio, E., Brayer, C., Cognet, G., Haquet, J.-F., Jégou, C., et al. (2003). Ex-vessel Corium Spreading: Results from the VULCANO Spreading Tests. *Nucl. Eng. Des.* 223, 75–102. doi:10.1016/s0029-5493(02)00397-7

Journeau, C., Bouyer, V., Charollais, F., Chikhi, N., Delacroix, J., Denoix, A., et al. (2022). Upgrading the PLINIUS Platform toward Smarter Prototypic-Corium Experimental R&D. *Nucl. Eng. Des.* 386, 111511. doi:10.1016/j.nucengdes.2021.111511

Journeau, C., Brayer, C., and Piluso, P. (2005). "Uncertainties on Thermodynamic and Physical Properties DataBases for Severe Accidents and Their Consequences on Safety Calculations [Report]," in *Tech. Rep. / OECD Workshop on Evaluation of Uncertainties in Relation to Severe Accidents and Level 2 PSA* (Aix en Provence, France.

Kim, C. S. (1975). Thermophysical Properties of Stainless Steels. Argonne National Lab, United States, ANL-75-55.

Korobeinikov, I., Chikhi, N., Fouquart, P., Turquais, B., Delacroix, J., Seetharaman, S., et al. (2021). Surface Tension and Density of Cr–Mn–Ni Steels with Transformation Induced Plasticity Effect [Journal]. *Steel Res. Int.* 92, 2000260.

Le Tellier, R., Saas, L., and Bajard, S. (2015). Transient Stratification Modelling of a Corium Pool in a LWR Vessel Lower Head. *Nucl. Eng. Des.* 287, 68–77. doi:10.1016/j.nucengdes.2015.02.009

Ma, W., Yuan, Y., and Sehgal, B. R. (2016). In-Vessel Melt Retention of Pressurized Water Reactors: Historical Review and Future Research Needs. *Engineering* 2, 103–111. - ISSN: 2095-8099. doi:10.1016/j.eng.2016.01.019

Matsumoto, T., Misono, T., Fujii, H., and Nogi, K. (2005). Surface Tension of Molten Stainless Steels under Plasma Conditions. *J. Mater Sci.* 40, 2197–2200. doi:10.1007/s10853-005-1932-9

Mills, K. C., and Brooks, R. F. (1994). Measurements of Thermophysical Properties in High Temperature Melts. *Mater. Sci. Eng. A* 178, 77–81. doi:10.1016/0921-5093(94)90522-3

Nakayoshi, A., Rempe, J. L., Barrachin, M., Bottomley, D., Jacquemain, D., Journeau, C., et al. (2020). Review of Fukushima Daiichi Nuclear Power Station Debris Endstate Location in OECD/NEA Preparatory Study on Analysis of Fuel Debris (PreADES) Project. *Nucl. Eng. Des.* 369, 110857. - ISSN: 0029-5493. doi:10.1016/j.nucengdes.2020.110857

Pellegrini, M., Dolganov, K., Herranz, L. E., Bonneville, H., Luxat, D., Sonnenkalb, M., et al. (2016). Benchmark Study of the Accident at the Fukushima Daiichi NPS: Best-Estimate Case Comparison. *Nucl. Technol.* 196, 198–210. doi:10.13182/nt16-63

Pellegrini, M., Herranz, L., Sonnenkalb, M., Lind, T., Maruyama, Y., Gauntt, R., et al. (2020). Main Findings, Remaining Uncertainties and Lessons Learned from the OECD/NEA BSAF Project. *Nucl. Technol.* 206, 1449–1463. doi:10.1080/00295450.2020.1724731

Pellegrini, M., Journeau, C., Seiler, N., Herranz, L. E., Bocanegra, R., Spengler, C., et al. (2022). "Analytical Benchmark on the Long Term Interaction of Molten Core and Dry Concrete at Fukushima Daiichi Unit 1 [Conference]," in Accepted by Nureth-19 Int. Top. Mtg. Nucl. React., Brussels (Brussels: Thermal Hydraulics).

Piluso, P., Adorni, M., Azarian, G., Bang, K.-H., Basu, S., Buck, M., et al. (2017). Status Report on Ex-Vessel Steam Explosion: EVSE, NEA-OECD.

Rempe, J. L., Knudson, D. L., Allison, C. M., Thinnes, G. L., and Atwood, C. L. (1997). Potential for AP600 In-Vessel Retention Through Ex-Vessel Flooding. Idaho National Engineering and Environmental Laboratory, Technical Evolution Report, INEEL/EXT-97-00779.

Saas, L., Tellier, R. L., and Skrzypek, E. (2017). "Rayleigh-Bénard and Bénard-Marangoni Convection in a Thin Metallic Layer on Top of Corium Pool," in The 8th European Review Meeting on Severe Accident Research – ERMSAR-2017, Warsaw, Poland.

Sangiorgi, M. (2015). In-Vessel Melt Retention (IVMR) Analyses of a VVER-1000 NPP. 6th ASTEC User's Club/2nd CESAM Workshop.

Seiler, J. M., Tourniaire, B., Defoort, F., and Froment, K. (2007). Consequences of Material Effects on In-Vessel Retention. *Nucl. Eng. Des.* 237, 1752–1758. doi:10.1016/j.nucengdes.2007.03.007

Song, J. (2021). Perspectives on a Severe Accident Consequences-10 Years after the Fukushima Accident. *J. Nucl. Eng.* 2, 398–411. doi:10.3390/jne2040030

Thakre, S. (2015). *On Fuel Coolant Interactions and Debris Coolability in Light Water Reactors [Report*. Ph.D. dissertation. Stockholm, Sweden: KTH.

Theofanous, T. G., Liu, C., Additon, S., Angelini, S., Kymäläinen, O., and Salmassi, T. (1997). In-vessel Coolability and Retention of a Core Melt. *Nucl. Eng. Des.* 169, 1–48. doi:10.1016/s0029-5493(97)00009-5

Tsurikov, D. (2007). *MASCA2 Project: Major Activities and Results [Report]*. Cadarache, France: Tech. rep. / Material scaling seminar.

Zanella, R., Tellier, R. L., Plapp, M., Tegze, G., and Henry, H. (2021). Three-dimensional Numerical Simulation of Droplet Formation by Rayleigh-Taylor Instability in Multiphase Corium. *Nucl. Eng. Des.* 379, 111177. doi:10.1016/j.nucengdes.2021.111177

Zhang, Y. P., Qiu, S. Z., Su, G. H., and Tian, W. X. (2011). A Simple Novel Analysis Procedure for IVR Calculation in Core-Molten Severe Accident. *Nucl. Eng. Des.* 241, 4634–4642. - The18th International Conference on Nuclear Engineering (ICONE-18). - ISSN: 0029-5493. doi:10.1016/j.nucengdes.2011.03.055

Conflict of Interest: The authors declare that the research was conducted in the absence of any commercial or financial relationships that could be construed as a potential conflict of interest.

Publisher's Note: All claims expressed in this article are solely those of the authors and do not necessarily represent those of their affiliated organizations, or those of the publisher, the editors, and the reviewers. Any product that may be evaluated in this article, or claim that may be made by its manufacturer, is not guaranteed or endorsed by the publisher.